g_A-driven shapes of electron spectra of forbidden β decays in the nuclear shell model

Joel Kostensalo* and Jouni Suhonen†
Department of Physics, University of Jyvaskyla, P.O. Box 35, FI-40014, Finland
(Received 10 May 2017; published 21 August 2017)

The evolution of the shape of the electron spectra of 16 forbidden β^- decays as a function of g_A was studied using the nuclear shell model in appropriate single-particle model spaces with established, well-tested nuclear Hamiltonians. The β spectra of ^{94}Nb$(6^+) \rightarrow {}^{94}Mo(4^+)$ and ^{98}Tc$(6^+) \rightarrow {}^{98}Ru(4^+)$ were found to depend strongly on g_A, which makes them excellent candidates for the determination of the effective value of g_A with the spectrum-shape method (SSM). A strong g_A dependence is also seen in the spectrum of ^{96}Zr$(0^+) \rightarrow {}^{96}Nb(6^+)$. This decay could be used for determining the quenching of g_A in sixth-forbidden decays in the future, when the measurement of the spectrum becomes experimentally feasible. The calculated shell-model electron spectra of the ground-state-to-ground-state decays of ^{87}Rb, ^{99}Tc, and ^{137}Cs and the decay of ^{137}Cs to the isomeric $11/2^-$ state in ^{137}Ba were found to be in excellent agreement with the spectra previously calculated using the microscopic quasiparticle-phonon model. This is further evidence of the robust nature of the SSM observed in the previous studies.

DOI: 10.1103/PhysRevC.96.024317

I. INTRODUCTION

At the nuclear level β decay can be considered as a mutual interaction of the hadronic and leptonic currents mediated by a massive vector boson $W^{\pm}$ [1]. The leptonic and hadronic currents can be expressed as a mixture of both vector and axial-vector components [2–4]. The weak vector and axial-vector coupling constants g_V and g_A enter the theory when the hadronic current is renormalized at the nucleon level [5]. The conserved vector-current hypothesis (CVC) and partially conserved axial-vector-current hypothesis (PCAC) yield the free-nucleon values $g_V = 1.00$ and $g_A = 1.27$ [6] but inside nuclear matter the value of g_A is affected by many-nucleon correlations and a quenched value might be needed to reproduce experimental data [1]. Precise information on the effective value of g_A is crucial when predicting half-lives of neutrinoless double beta decays since the half-lives are proportional to the fourth power of g_A [7,8].

The effective value of g_A has earlier been probed using a half-life comparison method, in which the predicted and experimental values are compared for different values of g_A. This has been done for Gamow-Teller and first-forbidden decays using nuclear matrix elements calculated with the proton-neutron quasiparticle random-phase approximation (pnQRPA) [9–13]. The half-life comparison method predicts that the value of g_A is quenched significantly in these transitions. Also in the old studies [14–17] of first-forbidden β decays, strong quenchings were predicted. In a recent shell-model study [18] of r-process waiting-point nuclei, a strong quenching of g_A was confirmed. The half-life comparison method could be used to find out if similar quenching of g_A is seen in highly forbidden unique beta decays by using the half-lives calculated in Ref. [19], once experimental data become available.

In Ref. [20] the spectrum-shape method (SSM) was introduced as a complementary way to study the effective value of the weak coupling constants. In the SSM the shapes of computed and experimental (normalized) electron spectra are compared in order to find the ratio g_A/g_V for nonunique forbidden beta β^- decays, for which the shape factors depend on g_A/g_V in a very nontrivial way. In Ref. [21] the SSM was applied to the fourth-forbidden ground-state-to-ground-state transition of ^{113}Cd using the microscopic quasiparticle-phonon model (MQPM) [22,23], the nuclear shell model (NSM) [24–26], the microscopic interacting boson-fermion model (IBFM-2) [27,28], and experimental spectrum of Ref. [29]. The closest match between the theoretical and experimental spectra was found when $g_A/g_V \approx 0.92$ for all three nuclear models. The half-life comparison method, on the other hand, gave very different results when different nuclear models were used. In Ref. [30] it was noticed that the shape of the spectrum was largely unaffected by modest changes in the MQPM wave function, even though the predicted half-life was affected significantly. The observations of these previous studies suggest that the SSM is very robust, quite insensitive to the details of the adopted nuclear mean field and Hamiltonian. It is thus a reliable tool for probing the ratio g_A/g_V.

The g_A-driven evolution of the shapes of several experimentally measurable forbidden nonunique decay spectra in medium-heavy odd-A nuclei was studied using the MQPM in Ref. [30]. Only four good candidates for the application of the spectrum-shape method have been found thus far. These are the ground-state-to-ground-state decays of ^{87}Rb, ^{99}Tc, ^{113}Cd, and ^{115}In [20,30]. In the present paper we set out to find potential new candidates for the application of the SSM in light to medium-heavy nuclei using the nuclear shell model. We also compare the NSM and MQPM β spectra of ^{87}Rb, ^{99}Tc, and ^{137}Cs to see if the model independence observed in Ref. [21] applies for these decays as well. The decays of ^{137}Cs to the $3/2^+$ ground state and the $11/2^-$ isomeric state of ^{137}Ba are particularly interesting for comparing the differences in the MQPM and NSM spectra, since the MQPM calculations predict a g_A-independent spectrum shape for these decays.

This article is organized as follows. In Sec. II we give the theoretical background behind the β spectrum shape. In

*joel.j.kostensalo@student.jyu.fi
†jouni.suhonen@phys.jyu.fi

Sec. III we describe the application of the nuclear shell model to the spectrum shape of forbidden β^- decays. In Sec. IV we present our results and in Sec. V we draw the conclusions.

II. THEORETICAL FORMALISM

We begin the description of the β^- decay by making the so-called impulse approximation, in which at the exact moment of decay the decaying nucleon only interacts via the weak interaction and the strong interaction with the other $A-1$ nucleons can be ignored. Since the vector boson W^- has a large mass and thus propagates only a short distance, the flow lines of the nucleons, i.e., the hadronic current, and the flow lines of the emitted leptons, i.e., the leptonic current, can be considered to interact at a pointlike weak-interaction vertex with an effective coupling constant $G_{\rm F}$, the Fermi constant. The parity nonconserving nature of the weak interaction is reflected in the fact that the hadronic current can be written at the quark level (up u and down d quarks) as a mixture of vector and axial-vector components as [2–4]

$$J_H^\mu = \bar{u}(x)\gamma^\mu(1-\gamma_5)d(x), \tag{1}$$

where γ^μ are the usual Dirac matrices and $\gamma_5 = i\gamma^0\gamma^1\gamma^2\gamma^3$. Renormalization effects of strong interactions must be taken into account when moving from the quark level to the hadron level. The hadronic current at the nucleon level (neutron n and proton p) can then be written as [5,6]

$$J_H^\mu = \bar{p}(x)\gamma^\mu(g_{\rm V} - g_{\rm A}\gamma_5)n(x), \tag{2}$$

where $g_{\rm V}$ and $g_{\rm A}$ are the weak vector and axial-vector coupling constants, respectively. The conserved vector-current hypothesis of the standard model (CVC) gives the free-nucleon value $g_{\rm V} = 1.0$ for the weak vector coupling constant and the partially conserved axial-vector-current hypothesis (PCAC) gives the free-nucleon value $g_{\rm A} = 1.27$ for the weak axial-vector coupling constant. Inside the nuclear matter the value of $g_{\rm A}$ is affected by many-nucleon correlations and so the free nucleon value might not be the one to use in practical calculations [6]. The present paper is a step towards solving the problem of what value to use for $g_{\rm A}$ inside finite nuclei.

In the impulse approximation the probability of the electron being emitted with kinetic energy between W_e and $W_e + dW_e$ is

$$P(W_e)dW_e = \frac{G_{\rm F}}{(\hbar c)^6}\frac{1}{2\pi^3\hbar}C(W_e) \times p_e c W_e (W_0 - W_e)^2 F_0(Z,W_e)dW_e, \tag{3}$$

where p_e is the momentum of the electron, Z is the proton number, $F_0(Z,W_e)$ is the Fermi function, and W_0 is the end-point energy of the β spectrum. The nuclear structure information is buried in the shape factor $C(w_e)$.

The half-life of a β decay can be written as

$$t_{1/2} = \frac{\kappa}{\tilde{C}}, \tag{4}$$

where $\tilde{C}$ is the integrated shape factor and the constant κ has the value [31]

$$\kappa = \frac{2\pi^3\hbar^7 \ln 2}{m_e^5 c^4 (G_{\rm F}\cos\theta_{\rm C})^2} = 6147\ {\rm s}, \tag{5}$$

$\theta_{\rm C}$ being the Cabibbo angle. In order to simplify the formalism it is usual to introduce unitless kinematic quantities $w_e = W_e/m_e c^2$, $w_0 = W_0/m_e c^2$, and $p = p_e c/(m_e c^2) = \sqrt{w_e^2 - 1}$. With the unitless quantities the integrated shape factor can be expressed as

$$\tilde{C} = \int_1^{w_0} C(w_e) p w_e (w_0 - w_e)^2 F_0(Z,w_e) dw_e. \tag{6}$$

The shape factor $C(w_e)$ of Eq. (6) contains complicated combinations of both (universal) kinematic factors and NMEs. In this paper we use the nuclear shell model to calculate the one-body transition densities related to the NMEs of the shape factor. The details of the shape factor and the constitution of its NMEs can be found from Refs. [32,33]. As in the previous SSM studies [20,21,30] we go beyond the earlier studies [32,33] and take into account the next-to-leading-order

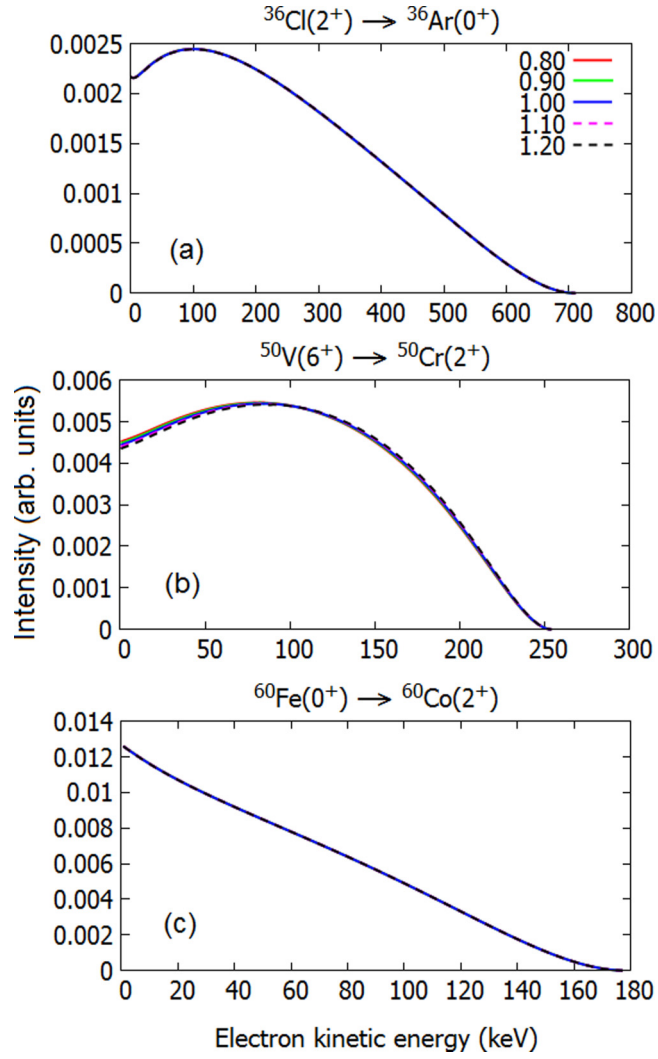

FIG. 1. Normalized electron spectra for the second-forbidden nonunique β^- decays of ^{36}Cl [panel (a)] and ^{60}Fe [panel (c)], and the fourth-forbidden nonunique decay of ^{50}V [panel (b)]. The value $g_{\rm V} = 1.00$ was adopted and the color coding represents the value of $g_{\rm A}$.

terms of the shape function. The details of the next-to-leading order shape factors are discussed in [21].

The shape factor $C(w_e)$ can be decomposed into vector, axial-vector, and mixed vector-axial-vector parts. In this decomposition the shape factor is

$$C(w_e) = g_V^2 C_V(w_e) + g_A^2 C_A(w_e) + g_V g_A C_{VA}(w_e). \quad (7)$$

Integrating Eq. (7) over the electron kinetic energy, we get an analogous expression for the integrated shape factor

$$\tilde{C} = g_V^2 \tilde{C}_V + g_A^2 \tilde{C}_A + g_V g_A \tilde{C}_{VA}, \quad (8)$$

where the factors $\tilde{C}_i$ in Eq. (8) are just constants, independent of the electron energy.

III. ADOPTED MODEL SPACES AND NUCLEAR HAMILTONIANS

The electron spectra of 16 forbidden β^- transitions were calculated for different values of the coupling constant g_A using the nuclear matrix elements produced by the nuclear shell model. The calculations were done using the shell model code NuShellX@MSU [34], with appropriate model spaces and well established Hamiltonians chosen for each studied decay individually. No additional truncations, beyond those used in the original works, were introduced. The calculations were run on a desktop computer with a 3.3 GHz processor, so the computational burden had to be taken into account when choosing the model space.

The adopted model spaces and Hamiltonians are as follows. *sd shell*: for the calculation of the wave functions and one-body transition densities related to the decay ^{36}Cl(2^+) → ^{36}Ar(0^+) we adopted the $0d$–$1s$ model space and the phenomenological USDB interaction [35]. *pf shell*: as in the earlier shell-model studies regarding the half-lives of the transitions ^{48}Ca(0^+) → ^{48}Sc(4^+,5^+,6^+) [36] and ^{50}V(6^+) → ^{50}Cr(2^+) [37], the $0f$–$1p$ model space with the interaction GXPF1A [38,39] was used to calculate the electron spectra of these decays. The GXPF1A interaction is very good at predicting the properties of pf-shell nuclei. However, since the computational burden increases dramatically when the number of particles approaches half of the maximum in the valence space, this interaction could not be used for the ^{60}Fe(0^+) → ^{60}Co(2^+) decay transition. Instead, a model space spanning the $\pi 0f_{7/2}$, $\nu 1p_{3/2}$, $\nu 0f_{5/2}$, and $\nu 1p_{1/2}$ orbitals was adopted with the Horie-Ogawa interaction [40,41]. $pfg_{9/2}$ *shell*: the jj44b interaction developed by Brown and Lisetskiy for the $0f_{5/2} - 1p - 0g_{9/2}$ model space (see endnote on Ref. [28] of [42]) was used for the calculation of the ^{87}Rb($3/2^-$) → ^{87}Sr($9/2^+$) transition. For the decays of the $A = 94$–99 nuclei, the effective interaction of Gloeckner [43] in the model space spanning the $\pi 1p_{1/2}$, $\pi 0g_{9/2}$, $\nu 2s_{1/2}$, and $2d_{5/2}$ was used. $sdgh_{11/2}$ *shell*: finally, for the decay transitions ^{126}Sn(0^+) → ^{126}Sb(2^+) and ^{137}Cs($7/2^+$) → ^{137}Ba($11/2^-$,$3/2^+$) the Sn100pn interaction [44] in the $0g_{7/2}2s1d0h_{11/2}$ model space was adopted.

IV. RESULTS AND DISCUSSION

Below we present our results: the electron spectra of 16 forbidden β^- decays (Figs. 1–5) and their integrated shape factors (Table I). The electron spectra are discussed in Sec. IV A and the integrated shape factors in Sec. IV B.

A. Electron spectra and the effective value of g_A

The studied spectra fall into three groups.

GROUP 1. The first group, for which the spectra can be found in Figs. 1 and 2, consists of six transitions for which the SSM analysis has not been done prior to this study. These decays are potentially interesting for the practical application of the spectrum-shape method, since most of them are second-forbidden nonunique transitions with branching ratios above 90%. The only exception is the undetected fourth-forbidden β^- decay branch of ^{50}V, for which the branching ratio has

TABLE I. Unitless integrated shape functions $\tilde{C}$ of the studied transitions and their vector $\tilde{C}_V$, axial-vector $\tilde{C}_A$, and mixed components $\tilde{C}_{VA}$. For the total integrated shape factor $\tilde{C}$ the values of the coupling constants were set to $g_V = g_A = 1.0$.

Transition	Type	$\tilde{C}_V$	$\tilde{C}_A$	$\tilde{C}_{VA}$	$\tilde{C}$
^{137}Cs($7/2^+$) → ^{137}Ba($11/2^-$)	1st uniq.	9.681×10^{-11}	8.322×10^{-6}	3.761×10^{-8}	8.359×10^{-6}
^{36}Cl(2^+) → ^{36}Ar(0^+)	2nd nonuniq.	6.081×10^{-9}	3.152×10^{-10}	-2.746×10^{-9}	3.650×10^{-9}
^{60}Fe(0^+) → ^{60}Co(2^+)	2nd nonuniq.	2.347×10^{-13}	5.232×10^{-11}	-7.000×10^{-12}	4.556×10^{-11}
^{94}Nb(6^+) → ^{94}Mo(4^+)	2nd nonuniq.	1.598×10^{-8}	1.469×10^{-8}	-3.058×10^{-8}	1.029×10^{-10}
^{98}Tc(6^+) → ^{98}Ru(4^+)	2nd nonuniq.	2.723×10^{-8}	2.544×10^{-8}	-5.254×10^{-8}	1.207×10^{-10}
^{99}Tc($9/2^+$) → ^{99}Ru($5/2^+$)	2nd nonuniq.	2.240×10^{-9}	2.130×10^{-9}	-4.361×10^{-9}	8.777×10^{-12}
^{126}Sn(0^+) → ^{126}Sb(2^+)	2nd nonuniq.	1.422×10^{-8}	7.125×10^{-9}	2.011×10^{-8}	4.145×10^{-8}
^{137}Cs($7/2^+$) → ^{137}Ba($3/2^+$)	2nd nonuniq.	4.211×10^{-6}	2.836×10^{-6}	6.879×10^{-6}	1.392×10^{-5}
^{87}Rb($3/2^-$) → ^{87}Sr($9/2^+$)	3rd nonuniq.	1.185×10^{-13}	2.082×10^{-14}	-9.734×10^{-14}	4.202×10^{-14}
^{48}Ca(0^+) → ^{48}Sc(4^+)	4th nonuniq.	8.946×10^{-28}	5.934×10^{-29}	-4.606×10^{-28}	4.934×10^{-28}
^{50}V(6^+) → ^{50}Cr(2^+)	4th nonuniq.	1.024×10^{-23}	9.137×10^{-25}	2.131×10^{-24}	1.329×10^{-23}
^{96}Zr(0^+) → ^{96}Nb(4^+)	4th nonuniq.	3.176×10^{-27}	3.170×10^{-28}	-2.006×10^{-27}	1.486×10^{-27}
^{48}Ca(0^+) → ^{48}Sc(5^+)	4th uniq.	2.577×10^{-30}	3.931×10^{-25}	1.334×10^{-27}	3.945×10^{-25}
^{96}Zr(0^+) → ^{96}Nb(5^+)	4th uniq.	1.765×10^{-29}	1.551×10^{-24}	6.844×10^{-27}	1.558×10^{-24}
^{48}Ca(0^+) → ^{48}Sc(6^+)	6th nonuniq.	1.124×10^{-32}	3.498×10^{-34}	3.947×10^{-33}	1.554×10^{-32}
^{96}Zr(0^+) → ^{96}Nb(6^+)	6th nonuniq.	5.811×10^{-33}	7.494×10^{-33}	-1.318×10^{-32}	1.234×10^{-34}

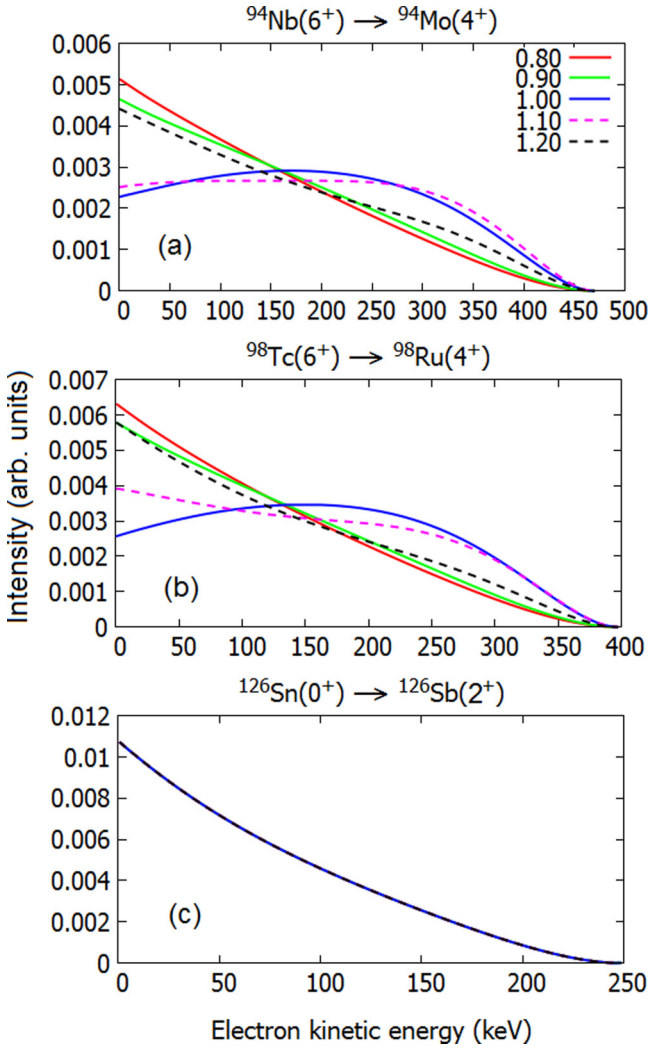

FIG. 2. Same as Fig. 1 but for the second-forbidden nonunique decays of ^{94}Nb [panel (a)], ^{98}Tc [panel (b)], and ^{126}Sn [panel (c)].

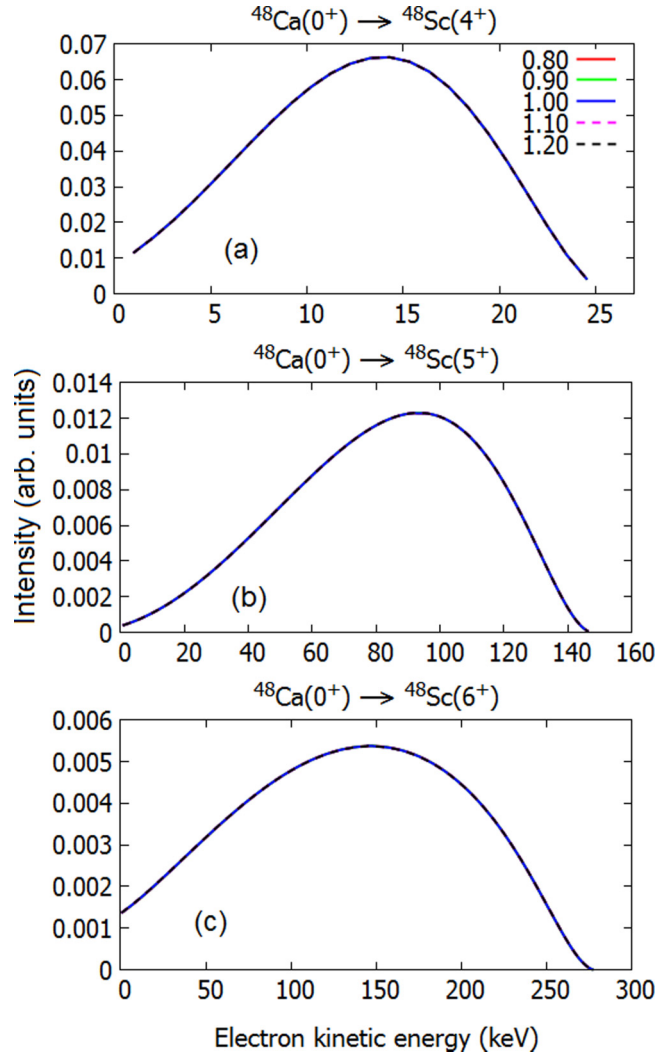

FIG. 3. Same as Fig. 1 but for the decays ^{48}Ca(0^+) → ^{48}Sc(4^+,5^+,6^+) [panels (a), (b), and (c)].

been predicted to be ≈2% by a recent shell-model calculation [36]. An earlier study [30] of the g_A-driven evolution of the electron spectra of odd-A nuclei demonstrated that the second and especially the fourth-forbidden nonunique β-decay spectra depend strongly on the effective value of the weak axial-vector coupling constant.

GROUP 2. The second group consists of the fourth-to-sixth-forbidden decays ^{48}Ca(0^+) → ^{48}Sc(4^+,5^+,6^+) and ^{96}Zr(0^+) → ^{96}Nb(4^+,5^+,6^+), for which the beta spectra are presented in Figs. 3 and 4. The decays of ^{48}Ca and ^{96}Zr appear to be dominated by the two-neutrino double beta decay mode [36,45,46], so the study of these decays is somewhat challenging experimentally. However, they can shed light on whether the spectra of highly forbidden beta decays are g_A dependent or not.

GROUP 3. The third group consists of four decays: ^{137}Cs($7/2^+$) → ^{137}Ba($11/2^-$,$3/2^+$), ^{99}Tc($9/2^+$) → ^{99}Ru($5/2^+$), and ^{87}Rb($3/2^-$) → ^{87}Sr($9/2^+$). The electron spectra of these decays was studied previously in [30] using the MQPM. The spectra of the ^{137}Cs decays were found to be independent of the value of g_A, while the dependence was significant for ^{87}Rb and ^{99}Tc. The shell-model and MQPM spectra of these decays are compared in order to see if the previously observed model independence of ^{113}Cd and ^{115}In spectra [21] holds also for these decays.

The spectra presented in Figs. 1 and 2 (GROUP 1) fall into two subgroups. The spectra of ^{36}Cl, ^{50}V, and ^{60}Fe [Fig. 1, panels (a), (b), and (c)], and ^{126}Sn [Fig. 2, panel (c)] do not exhibit noticeable dependence on the value of the axial-vector coupling constant. This is very surprising since the decay of ^{50}V is fourth forbidden, and all the seven studied fourth-forbidden decays in Ref. [30] depend heavily on g_A. The spectra of the second subgroup, ^{94}Nb and ^{98}Tc [Fig. 2, panels (a) and (b)], are significantly g_A dependent. The g_A driven evolution of the spectra is not only very similar for these two decays, but also nearly identical to the one of ^{99}Tc, shown in Fig. 5, panel (c), even though the Q value of these decays varies between 300 keV and 450 keV. A similar grouping phenomenon was seen for several decays in [30]: for example the shapes of the spectra of fourth-forbidden

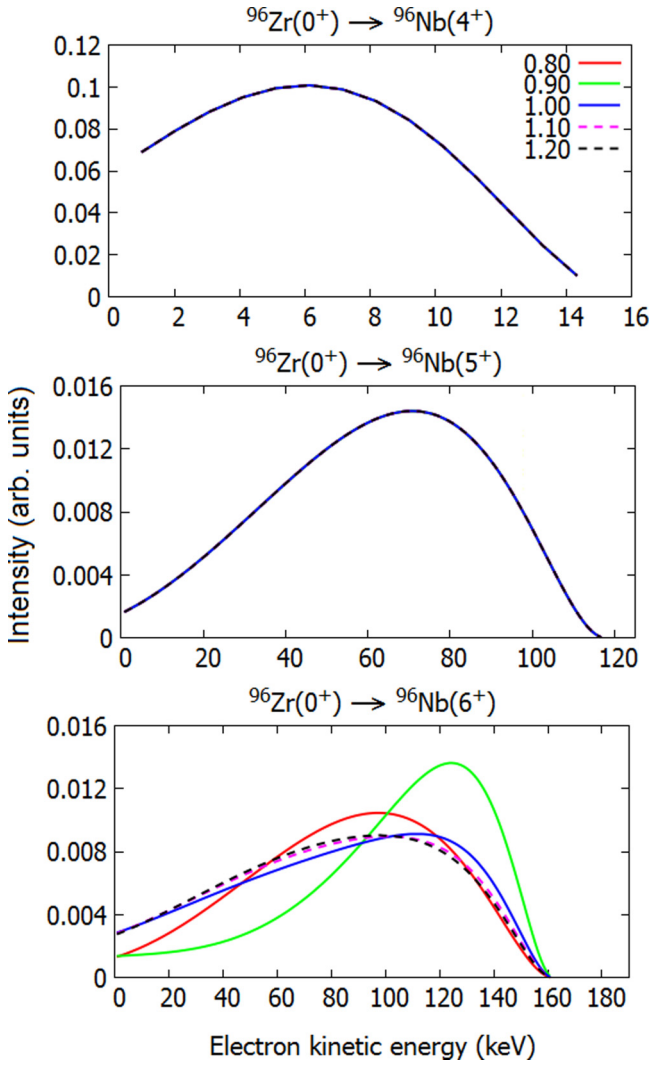

FIG. 4. Same as Fig. 1 but for the decays ^{96}Zr(0^+) → ^{96}Nb(4^+,5^+,6^+) [panels (a), (b), and (c)].

ground-state-to-ground-state β^- decays of ^{97}Zr, ^{101}Mo, ^{117}Cd, and ^{119}In have an almost identical g_A evolution.

Decays of GROUP 2, ^{48}Ca(0^+) → ^{48}Sc(4^+,5^+,6^+) and ^{96}Zr(0^+) → ^{96}Nb(4^+,5^+,6^+), were studied in order to see if there appears some interesting systematic behavior. Since the shape of the spectra of fourth-forbidden nonunique decays of odd-A nuclei depends on g_A in a significant way, it is interesting to see if this holds for the even-A nuclei. Since the spectrum on ^{50}V is largely independent of the values of the weak coupling constants, the dependence is not strong for at least some fourth-forbidden decays. The shape of the electron spectra of ^{48}Ca(0^+) → ^{48}Sc(4^+,5^+,6^+) and ^{96}Zr(0^+) → ^{96}Nb(4^+,5^+) transitions is independent of g_A, as shown in Fig. 3, panels (a), (b), and (c) and in Fig. 4, panels (a) and (b), revealing a second exception, ^{48}Ca(0^+) → ^{48}Sc(4^+), to the g_A-dependent fourth-forbidden nonunique decays. The sixth-forbidden decay ^{96}Zr(0^+) → ^{96}Nb(6^+) [Fig. 4, panel (c)], on the other hand, exhibits a strong g_A dependence. The evolution is very different from the one of the ^{94}Nb and ^{98}Tc [Fig. 2, panels (a) and (b)], and ^{99}Tc [Fig. 5, panel (c)] studied in the present paper and the fourth-forbidden ones studied in [30]. The branching ratio is, however, so small that the measurement of this spectrum is not currently within reach of experiments. It is somewhat striking that, from the 38 different forbidden decays studied in the present paper and in Ref. [30], strong g_A dependence is seen only in even-forbidden decays.

In Fig. 5 the shell-model and MQPM spectra of the experimentally interesting decays found in Ref. [30] are shown for comparison. For ^{87}Rb [panels (a) and (b)], which is the best candidate for the determination of the quenching of g_A in third-forbidden decays, the MQPM and shell-model spectra are practically identical. For ^{99}Tc [panels (c) and (d)] the evolution predicted by the two models is also similar, but in the range $g_A = 0.9$–1.1 there is some difference in the shape, leading to a potential small uncertainty in the value of g_A when comparing to the experimental spectrum, hopefully available in the (near) future. The two studied decays of ^{137}Cs [panels (e) and (f)] were found to be g_A independent when using the MQPM model in Ref. [30]. The shell-model spectra calculated for these decays were not only also g_A independent, but overlap with the MQPM spectra perfectly. Measurements of these spectra would by very desirable, since they would shed light on the quality of the calculated spectra, independent of the chosen nuclear model.

B. Integrated shape factor $\tilde{C}$

The integrated shape factors $\tilde{C}$ and their decomposition to the components of Eq. (8) are presented in Table I. For all the studied decays the sign of the vector and axial-vector components is positive and the sign of the mixed vector-axial-vector component varies. For the second-forbidden nonunique decays of ^{94}Nb and ^{98,99}Tc which have very similar spectrum-shape evolution, the vector- and axial-vector components are roughly equal and the vector-axial-vector component is roughly twice as large, but with a negative sign. The resulting total integrated shape factor is two magnitudes smaller than its components. For the sixth-forbidden decay ^{96}Zr(0^+) → ^{96}Nb(6^+) the axial-vector component is 30% larger than the vector component and the vector-axial-vector component is again roughly the sum of the two other components and negative in sign.

For ^{87}Rb the decomposition is similar to the case of the MQPM: the vector component $\tilde{C}_V$ is the largest, the axial-vector component $\tilde{C}_A$ is about 20% of $\tilde{C}_V$, and the vector-axial-vector component $\tilde{C}_{VA}$ is the smallest and has a negative sign. However, the components and the total integrated shape factor are approximately 30% larger for the MQPM. In the case of ^{99}Tc the difference is much larger and the MQPM results are roughly twice the shell model ones. For the two studied decays of ^{137}Cs there is no g_A dependence. The decay to the isomeric $11/2^-$ state is unique and thus (practically) g_A independent. On the other hand, the decay to the $3/2^+$ ground state is nonunique but g_A independent since the three components of $\tilde{C}$ have the same sign and no interference between the components occurs. For these two decays the normalized shell model and MQPM electron spectra overlap perfectly but the difference in $\tilde{C}$ is considerable. Again, the relative fractional decomposition is almost identical for the two nuclear models, but the absolute

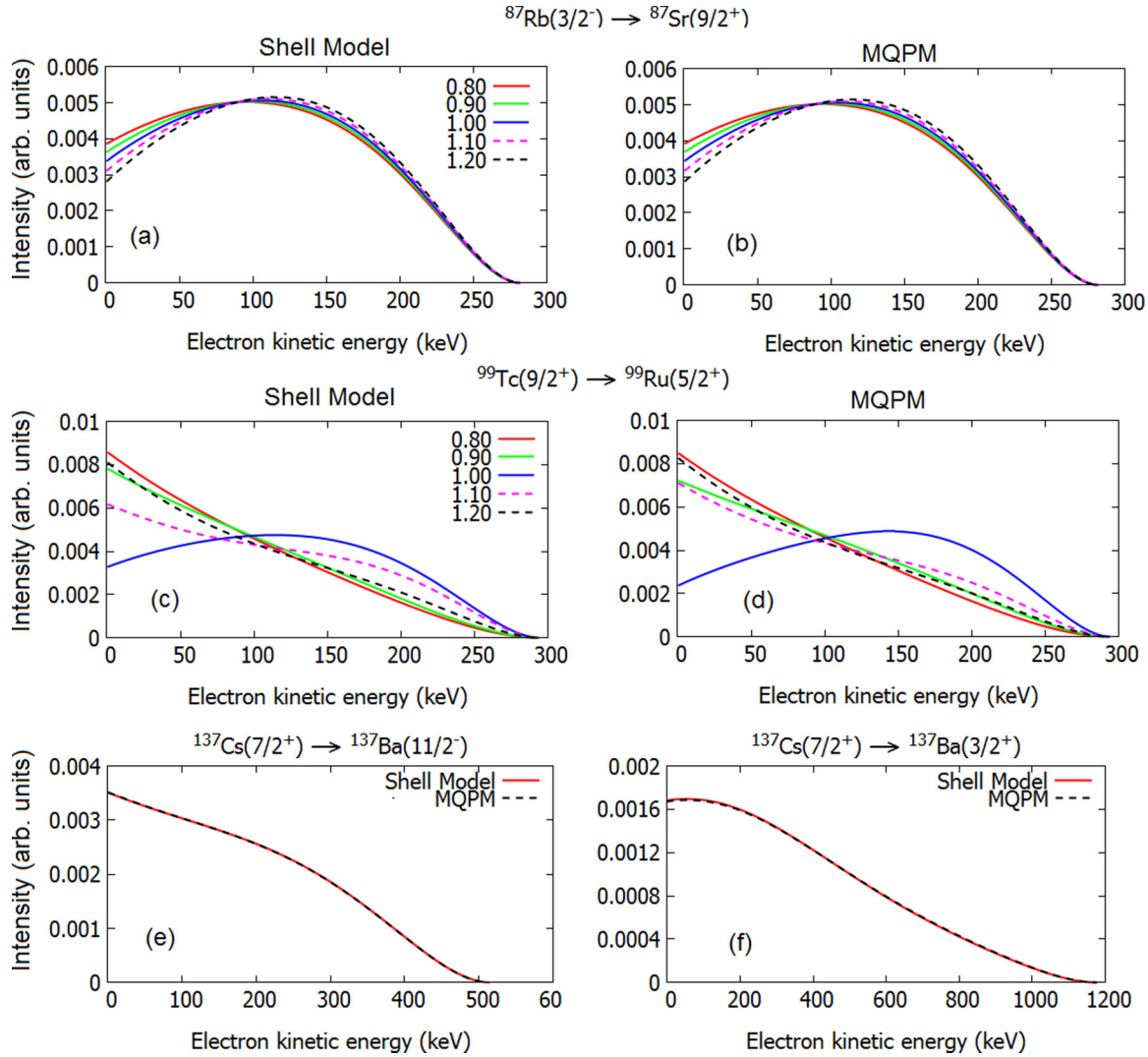

FIG. 5. Presently calculated shell-model spectra and the MQPM spectra, first published in Ref. [30], for the ground-state-to-ground-state decays of ^{87}Rb [panels (a) and (b)], ^{99}Tc [panels (c) and (d)], and ^{137}Cs [panel (f)], and the decay of ^{137}Cs to the isomeric $11/2^-$ state in ^{137}Ba [panel (e)]. The color coding in the spectra of ^{87}Rb and ^{99}Tc refers to the value of g_A. The shape of the electron spectra of the two ^{137}Cs decays is g_A independent, and the color coding in these decays refers to the adopted nuclear model. The free-nucleon value $g_V = 1.00$ was used in all calculations.

value of the MQPM $\tilde{C}$ is 40-fold the shell model one for the decay to the $11/2^-$ state, and 8-fold for the decay to the $3/2^+$ state. Due to the $\tilde{C}^{-1}$ dependence of the half-life, the half-lives predicted by the two models do not agree with each other at all. This is a strong indication that the spectrum-shape method is a more robust tool for determining the effective value of g_A than just a simple half-life comparison.

V. CONCLUSIONS

The evolution of the electron-spectrum shapes of 16 forbidden β^- decays, driven by the value of the axial-vector coupling constant g_A, were studied using nuclear matrix elements derived from the nuclear shell model. Established and well-tested nuclear Hamiltonians were used in these investigations. In the β-decay shape factors the usually omitted next-to-leading-order terms were taken into account. The main objective of the study was to find experimentally detectable transitions for which the shape of the electron spectra depends sensitively on the value of the weak coupling constants. Comparing the calculated and measured spectra the effective value of g_A can be extracted.

The electron spectra of ^{94}Nb$(6^+) \rightarrow$ ^{94}Mo(4^+) and ^{98}Tc$(6^+) \rightarrow$ ^{98}Ru(4^+) depend significantly on the effective value of g_A and these transitions are thus excellent new candidates for the spectrum-shape method (SSM). Both of these decays have almost a 100% branching ratio, and have been experimentally observed. The shell-model spectra of the previously found candidates, the ground-state-to-ground-state decays of ^{87}Rb and ^{99}Tc, agree well with the microscopic quasiparticle-phonon model predicted spectra of a previous study, which makes the experimental measurement of these spectra very desirable. The g_A-independent shell model and MQPM spectrum shapes of the

^{137}Cs$(7/2^+) \rightarrow$ ^{137}Ba$(11/2^-,3/2^+)$ transitions overlap perfectly. The measurement of these spectra would shed light on the quality of the calculated spectra.

The transitions for which a heavy g_A dependence has been recorded thus far are all even forbidden. Unlike in the case of the fourth-forbidden transitions in odd-A nuclei studied in Ref. [30], which all showed a strong g_A dependence, such a dependence is not seen in the corresponding transitions in the studied even-A nuclei. Thus far all the found transitions with a very strongly g_A-dependent spectrum shape are in the mass region $A = 94$–119. Most of the experimentally accessible forbidden nonunique transitions in odd-A nuclei with $A \leqslant 169$ and second or higher-forbidden nonunique transitions in even-A nuclei with $A \leqslant 98$ have now been studied. The potential new candidates for the spectrum-shape method are heavier, and the study of these decays requires the adoption of some other nuclear model due to the large computational burden and the other problems with shell-model calculations for heavy deformed nuclei.

ACKNOWLEDGMENTS

This work has been partially supported by the Academy of Finland under the Finnish Centre of Excellence Programme 2012-2017 (Nuclear and Accelerator Based Programme at JYFL).

[1] J. Suhonen, *From Nucleons to Nucleus: Concepts of Microscopic Nuclear Theory* (Springer, Berlin, 2007).
[2] R. P. Feynmann and M. Gell-Mann, Phys. Rev. **109**, 193 (1958).
[3] R. P. Feynmann and M. Gell-Mann, Phys. Rev. **111**, 362 (1958).
[4] W. Theis, Z. Phys. **150**, 590 (1958).
[5] K. Zuber, *Neutrino Physics* (Institute of Physics Publishing Ltd., London, 2004).
[6] E. D. Commins, *Weak Interactions* (McGraw-Hill, New York, 2007).
[7] J. Suhonen and O. Civitarese, Phys. Rep. **300**, 123 (1998).
[8] J. Maalampi and J. Suhonen, Adv. High Energy Phys. **2013**, 505874 (2013).
[9] H. Ejiri and J. Suhonen, J. Phys. G: Nucl. Part. Phys. **42**, 055201 (2015).
[10] H. Ejiri, N. Soukouti, and J. Suhonen, Phys. Lett. B **729**, 27 (2014).
[11] P. Pirinen and J. Suhonen, Phys. Rev. C **91**, 054309 (2015).
[12] D. S. Delion and J. Suhonen, Europhys. Lett. **107**, 52001 (2014).
[13] F. F. Deppisch and J. Suhonen, Phys. Rev. C **94**, 055501 (2016).
[14] E. K. Warburton, Phys. Rev. C **42**, 2479 (1990).
[15] E. K. Warburton, Phys. Rev. C **44**, 233 (1991).
[16] E. K. Warburton, I. S. Towner, and B. A. Brown, Phys. Rev. C **49**, 824 (1994).
[17] E. K. Warburton and I. S. Towner, Phys. Rep. **242**, 103 (1994).
[18] Q. Zhi, E. Caurier, J. J. Cuenca-García, K. Langanke, G. Martínez-Pinedo, and K. Sieja, Phys. Rev. C **87**, 025803 (2013).
[19] J. Kostensalo and J. Suhonen, Phys. Rev. C **95**, 014322 (2017).
[20] M. Haaranen, P. C. Srivastava, and J. Suhonen, Phys. Rev. C **93**, 034308 (2016).
[21] M. Haaranen, J. Kotila, and J. Suhonen, Phys. Rev. C **95**, 024327 (2017).
[22] J. Toivanen and J. Suhonen, J. Phys. G. **21**, 1491 (1995).
[23] J. Toivanen and J. Suhonen, Phys. Rev. C **57**, 1237 (1998).
[24] B. H. Wildenthal, M. S. Curtin, and B. A. Brown, Phys. Rev. C **28**, 1343 (1983).
[25] G. Martínez-Pinedo, A. Poves, E. Caurier, and A. P. Zuker, Phys. Rev. C **53**, R2602(R) (1996).
[26] E. Caurier, F. Nowacki, and A. Poves, Phys. Lett. B **711**, 62 (2012).
[27] F. Iachello and A. Arima, *The Interacting Boson Model* (Cambridge University Press, Cambridge, UK, 1987).
[28] F. Iachello and P. V. Isacker, *The Interacting Boson-Fermion Model* (Cambridge University Press, New York, 1991).
[29] P. Belli, R. Bernabei, N. Bukilic, F. Cappella, R. Cerulli, C. J. Dai, F. A. Danevich, J. R. de Laeter, A. Incicchitti, V. V. Kobychev, S. S. Nagorny, S. Nisi, F. Nozzoli, D. V. Poda, D. Prosperi, V. I. Tretyak, and S. S. Yurchenko, Phys. Rev. C **76**, 064603 (2007).
[30] J. Kostensalo, M. Haaranen, and J. Suhonen, Phys. Rev. C **95**, 044313 (2017).
[31] J. C. Hardy, I. S. Towner, V. Koslowsky, E. Hagberg, and H. Schmeing, Nucl. Phys. A **509**, 429 (1990).
[32] H. Behrens and W. Bühring, *Electron Radial Wave Functions and Nuclear Beta Decay* (Clarendon, Oxford, 1982).
[33] M. T. Mustonen, M. Aunola, and J. Suhonen, Phys. Rev. C **73**, 054301 (2006).
[34] B. A. Brown and W. D. M. Rae, Nucl. Data Sheets **120**, 115 (2014).
[35] B. A. Brown and W. A. Richter, Phys. Rev. C **74**, 034315 (2006).
[36] M. Haaranen, M. Horoi, and J. Suhonen, Phys. Rev. C **89**, 034315 (2014).
[37] M. Haaranen, P. C. Srivastava, J. Suhonen, and K. Zuber, Phys. Rev. C **90**, 044314 (2014).
[38] M. Honma, T. Otsuka, B. A. Brown, and T. Mizusaki, Phys. Rev. C **69**, 034335 (2004).
[39] M. Honma, T. Otsuka, B. A. Brown, and T. Mizusaki, Eur. Phys. J. A **25**, 499 (2005).
[40] H. Horie and K. Ogawa, Prog. Theor. Phys. **46**, 439 (1971).
[41] H. Horie and K. Ogawa, Nucl. Phys. A **216**, 407 (1973).
[42] B. Cheal, E. Mané, J. Billowes, M. L. Bissell, K. Blaum, B. A. Brown, F. C. Charlwood, K. T. Flanagan, D. H. Forest, C. Geppert, M. Honma, A. Jokinen, M. Kowalska, A. Krieger, J. Krämer, I. D. Moore, R. Neugart, G. Neyens, W. Nörtershäuser, M. Schug, H. H. Stroke, P. Vingerhoets, D. T. Yordanov, and M. Žáková, Phys. Rev. Lett. **104**, 252502 (2010).
[43] D. H. Gloeckner, Nucl. Phys. **A253**, 301 (1975).
[44] B. A. Brown, N. J. Stone, J. R. Stone, I. S. Towner, and M. Hjorth-Jensen, Phys. Rev. C **71**, 044317 (2005).
[45] H. Heiskanen, M. T. Mustonen, and J. Suhonen, J. Phys. G: Nucl. Part. Phys. **34**, 837 (2007).
[46] M. Alanssari, D. Frekers, T. Eronen, L. Canete, J. Dilling, M. Haaranen, J. Hakala, M. Holl, M. Ješkovský, A. Jokinen, A. Kankainen, J. Koponen, A. J. Mayer, I. D. Moore, D. A. Nesterenko, I. Pohjalainen, P. Povinec, J. Reinikainen, S. Rinta-Antila, P. C. Srivastava, J. Suhonen, R. I. Thompson, A. Voss, and M. E. Wieser, Phys. Rev. Lett. **116**, 072501 (2016).